Remote sensing-derived fractures and shrub patterns to identify groundwater dependence

E. Guirado[1,2*], D. Alcaraz-Segura[1,3,4], J.P. Rigol-Sánchez[2], J. Gisbert[2], F.J. Martínez-Moreno[5], J. Galindo-Zaldívar[5,6], L. González-Castillo[5] , J. Cabello[1,2*]

1 Andalusian Center for the Assessment and Monitoring of Global Change, University of Almería, 04120, Almería, Spain
2 Department of Biology and Geology, University of Almería, 04120, Almería, Spain
3 Department of Botany, University of Granada, Av. de Fuentenueva, s/n 18071, Granada, Spain
4 4iecolab. Interuniversitary Institute for Earth System Research (IISTA) – University of Granada, Av. del Mediterráneo, s/n, 18006, Granada, Spain
5 Department of Geodynamics, University of Granada, Av. de Fuentenueva, s/n, 18071, Granada, Spain
6 Andalusian Institute of Earth Sciences, CSIC-University of Granada, 18071, Granada, Spain

*Corresponding author. E-mail: e.guirado@ual.es; jcabello@ual.es

Running head: Detecting groundwater dependence from remote-sensing-derived fractures and vegetation patterns

This article has been accepted for publication and undergone full peer review but has not been through the copyediting, typesetting, pagination and proofreading process which may lead to differences between this version and the Version of Record. Please cite this article as doi: 10.1002/eco.1933

ABSTRACT

The identification and location of groundwater dependent ecosystems (GDEs) are the first steps in protecting and managing them. Such identifications are challenging where the surface expressions of groundwater are not obvious. This work presents a remote-sensing-based approach to infer the groundwater dependence of semi-arid shrubs from their association with fractures that facilitate root access to groundwater. As a case study, we used the *Ziziphus lotus* matorral in SE Spain, a priority conservation habitat in the European Union (Habitat 5220*, Directive 92/43/EEC) that is highly threatened by agricultural and urban sprawl. The approach combines object-based image analysis of high-resolution orthoimages to map *Ziziphus* individuals, geomorphometric analysis of a LiDAR-derived terrain model to map bedrock fractures, and spatial statistics to assess the association between *Ziziphus* and fractures. Electrical resistivity tomography was used to validate the identified fractures and the seasonal dynamics of the normalized difference vegetation index was used to prove that *Z. lotus* maintained higher greenness during the summer drought and was less coupled with precipitation than the nearby non-phreatophytic vegetation. A majority (61%) of the *Ziziphus* patches, particularly the smallest ones, occurred within 50 m of faults. This spatial association between phreatophyte shrubs and fractures contributes to the identification of GDEs. This approach offers several advantages since it is simple, low-cost, and non-destructive. In addition, the differentiation of shrubs into size classes provided insights into the long-term environmental controls underlying the establishment of *Ziziphus* individuals. The evidence of groundwater dependence by *Z. lotus* in habitat 5220* indicates the need for its urgent protection under the Water Framework Directive.

KEYWORDS: Average minimum distance; Cabo de Gata-Níjar Natural Park; phreatophyte; Sentinel-2A; shrub mapping; very-high-resolution images.

1. INTRODUCTION

Groundwater dependent ecosystems (GDEs; Eamus et al., 2006) provide multiple ecosystem services for humankind (Kløve et al., 2011); GDEs are globally at risk due to unsustainable groundwater extraction and climate change (e.g., Barron et al., 2012; Eamus et al., 2015; Kløve et al., 2011; Kløve et al., 2014a, 2014b; Naumburg et al., 2005). A critical step towards the conservation of GDEs is to improve our ability to detect them (Eamus et al., 2006; Howard and Merrifield 2010), which is a requirement that has been already considered even at major regulatory levels. For instance, that is the case for the European Water Framework Directive (WFD, 2000/60/EC), which obliges member states to first identify and inventory surface ecosystems associated with groundwater bodies, and second, to designate influence areas for their subsequent protection (Boulton, 2005; Kløve et al., 2014a). Thus, the development of cost-effective methods to identify and locate GDEs and to systematically characterize their dependence on groundwater emerges as an important step for their conservation and management (Barron et al., 2012; Münch and Conrad 2007; Brown et al., 2010).

The identification and monitoring of GDEs are often time-consuming and costly exercises that require a high level of technical expertise (Eamus et al., 2015). Although several methods have been implemented in this direction (Pérez-Hoyos et al., 2016, Eamus et al., 2015), the development of new ones is still challenging, particularly when there is no surface evidence of groundwater presence (UK TAG, 2012), or there are not enough data and tools to recognize hypothetical GDEs. Pérez-Hoyos et al. (2016) and Eamus et al. (2015) offer a profound review of field, remote sensing and GIS methods to identify and characterize groundwater dependent ecosystems. Some of these methods reveal the dependence on groundwater from the spatial relationship between phreatophytic vegetation and landforms

(Pérez-Hoyos et al., 2016). For instance, geological lineaments, fractures, and faults can often be associated with GDEs (Münch and Conrad 2007) since they may facilitate root access to groundwater (Colvin et al., 2003).

This may be the case of the arborescent semi-arid shrubland of *Ziziphus lotus* (L.) Lam. This ecosystem is protected under the European Habitats Directive (priority Habitat 5220*, 92/43/EEC), and it is one of the few terrestrial GDEs in European drylands. Changes in the quantity, quality, and distribution of groundwater affect GDEs especially in drylands (Murray et al., 2003). In Spain, *Ziziphus* shrublands can be affected by the decline in water-table levels due to the overexploitation of groundwater (García et al., 2003), as well as by its direct fragmentation and destruction due to greenhouse agriculture and urban sprawl (Tirado, 2009). Several traits indicate a strong dependence of *Z. lotus* on groundwater: 1) it has deep roots that can extend up to 15 m horizontally (Walter and Breckle, 1986) and 60 m vertically (Le Houérou, 2006), enabling the roots to reach groundwater; 2) it accumulates a relatively large biomass for dryland conditions, reaching heights up to 5.5 m, areas of 500 m^2, and bio-volumes of 900 m^3 (Rodríguez, 2016); 3) it extensively propagates vegetatively (Walter and Breckle, 1986); 4) it is a typical winter deciduous phreatophyte that maintains its vegetative growth throughout the Mediterranean summer drought (Gorai et al., 2010); and 5) it is a drought tolerant phreatophyte that reaches low water potentials during the driest months of the summer (Gorai et al., 2010).

This work proposes the use of remote sensing methods to map the spatial distributions of shrubs and fractures as a means to identify groundwater dependent ecosystems in drylands. Our guiding hypothesis was that groundwater dependence could be revealed through the spatial relationship between the distributions of shrubs and bedrock fractures that would

facilitate their access to groundwater. As a proof of concept, we used the spatial distributions of *Z. lotus* and fractures in a semi-arid plain where there is no surface evidence of groundwater presence. For this, we first mapped the shrubs using object-based image analysis (OBIA) of very high-resolution orthoimages and the fracture zones using digital elevation models derived from light detection and ranging (LiDAR), and then we assessed the overlap of the two maps. In addition, we used electrical resistivity tomography to validate the detection of fractures and the satellite-derived seasonal dynamics of vegetation greenness to show the *Z. lotus* growth during the dry season as a proof of groundwater dependence.

2. MATERIALS AND METHODS

2.1. STUDY AREA AND HYDROGEOLOGICAL FRAMEWORK

The study site is a semi-arid coastal plain (4.7 km^2), located in the Natural Park of Cabo de Gata-Níjar, Spain (36º49'43"N, 2º17'30"W) (Figure 1). The average annual temperature is 19 °C, annual rainfall is 200 mm, and annual potential evapotranspiration is 1390 mm (Oyonarte et al., 2012). The maximum altitude is 33 m a.s.l. and the slope is 2-3%. Geologically, it is composed of Quaternary deposits fractured by two major tectonic events that produced sinistral fractures oriented ≈N43ºE (sometimes with a vertical component) and normal faults oriented ≈N150ºE (Goy and Zazo, 1983, 1986; Sola et al., 2007). The lithology and stratigraphy are characterized by an upper-Miocene-Pliocene basal substrate on which 80 m of Pliocene-Quaternary conglomerates and sandstones settle. Frequently, there are also silts and clays interbedded with fractured calcareous crusts on the surface. The soil water retention capacity is extremely low because of its sandy-loam texture and very thin soil layer (Chamizo et al., 2015).

The local aquifer is coastal, shallow, free, and composed of gravel and sand deposits located in the discharge zone at the end of two wadis basins. Although it could be considered as SW extension of the main regional aquifer (Hornillo-Cabo de Gata), it is hydraulically separated by a major fault (Daniele et al., 2010). Consequently, recharge mainly comes from the limited local rainfall and negligibly comes from irrigation returns and nearby aquifers. Groundwater withdrawals for greenhouse irrigation have increased over the last few decades, causing a 30 m decline of the water-table in the main aquifer. As a result of such high withdrawals and low recharge, there is regional evidence of seawater intrusion (García et al., 2003).

The vegetation shows a typical structure of semi-arid formations with a matrix of annual grasses and small shrubs interrupted by small bare ground extensions and patches of arborescent shrubs (Rivas Goday and Bellot, 1944; Tirado and Pugnaire, 2003). These patches are dominated by *Z. lotus*, a large hemispherical thorny shrub that reaches up to 3-5 m in height and forms patches (*Ziziphus* patches hereafter) with average areas greater than 100 m^2. Its thorny structure and deep roots mark it as an ecosystem engineer that produces green biomass during the summer drought and uplifts water from the deep layers to the upper soil, thus acting as a "fertile island" refuge for many plant and animal species (Tirado and Pugnaire, 2003, 2005; Tirado, 2009; Lagarde et al., 2012).

2.2. WORKFLOW, DATASETS, AND GROUND TRUTH

To derive the dependence of the vegetation on groundwater from the spatial patterns of phreatophytic shrubs (Figure 2), we first mapped the spatial patterns of *Ziziphus* patches and fracture zones that could facilitate access to groundwater, and we then analysed their spatial relationship.

2.2.1. MAPPING *ZIZIPHUS LOTUS* PATCHES

The mapping of *Ziziphus* patches was based on the object-based image analysis (OBIA) of an aerial orthoimage and a normalized digital surface model. Both products were simultaneously obtained in August 2011 from a helicopter at an altitude of 550 m. The orthoimage was captured with an airborne RGB H4D Hasselblad camera with 50 megapixels and a 50 mm lens. Both images were orthorectified with a final spatial resolution of 10 cm. The surface model was derived from a high-density point cloud recorded with an airborne Riegl Q240i LMS LiDAR scanner system. The average point density was 4 points/m^2 (sufficient for the detection of both *Ziziphus* patches and fracture zones). The point cloud was classified into vegetation and ground classes. The vegetation elevation model was calculated as the difference between the digital surface model (ground and vegetation canopy elevations) and the digital terrain model (only ground elevations) at a spatial resolution of 1 m^2.

First, we partitioned the orthoimage and surface model into significant objects (segments or polygons) with similar characteristics in space, colour, and height (Hay and Castilla, 2006). For this, we optimized the effectiveness of the multiresolution algorithm in eCognition (v.8.9, Trimble) with 3240 combinations of three dimensionless parameters: "Shape", "Compactness" and "Scale" (Esch et al., 2008). Scale ranged from 100 to 200 in steps of 5, Shape and Compactness ranged from 0.1 to 0.9 in steps of 0.1, with and without hierarchy options (Burnett and Blaschke, 2003; Syed et al., 2005; Lang and Langanke, 2006). To identify the combination with segments that better corresponded to *Ziziphus* patches in the field, 200 ground-truth observations of *Ziziphus* patches (approximately 10% of the population) were digitized with a submetric GPS Leica GS20 in twelve systematic transects (2 km long each) parallel to the coastline (125 m gap between transects) (e.g., Liu et al., 2012; Witharana and Civco, 2014). The best segmentation had to meet two criteria: 1)

segments overlapped or were contained within the field-digitized polygons, and 2) the Euclidean distance v.2 (ED2) and the subsequent potential segmentation error (PSE) and number-of-segments ratio (NSR) (Table 4) were optimal (the closer to zero, the better) following Clinton et al. (2010) and Liu et al. (2012). According to Liu et al. (2012), ED2 values closer to zero indicate better geometric (contour) and arithmetic (surface) coincidence between the OBIA-obtained segments and the field-digitized polygons, while high ED2 values indicate a mismatch. The geometric accuracy is estimated by PSE (Eq. 1), where values closer to zero indicate a better fit between the OBIA segments and the field-digitized polygons, and greater PSE values indicate worse fits. The arithmetic accuracy is estimated by the NSR (Eq. 2), where values closer to zero indicate better coincidence between the OBIA segments and the field-digitized polygons, and greater NSR values indicate discrepancy.

Second, the best segmentation was classified into two classes: *Ziziphus* patches (Z class) and bare soil and sparse vegetation (S class) using the nearest neighbour classifier in Definiens software (2009). The segment features that were used for the classification were average brightness (red, green, and blue bands as the true colour image), area, roundness and grey-level co-occurrence matrix, which is one of the earliest techniques used for image texture analysis. The classification training and validation were based on 200 samples of *Ziziphus* patches and 200 samples of bare soil with sparse vegetation, which were selected randomly following longitudinal transects to the coast with a separation of 150 m between samples. We used 70% of the samples for training and 30% for validation. Validation was assessed by Hellden's mean accuracy and the kappa index on the error and confusion matrix (Cohen, 1968).

2.2.2. DETECTING LINEAMENTS BY GEOMORPHOMETRIC ANALYSIS

Since the geological maps were too coarse to locate fractures in the area, an "ad hoc" fracture map was developed from the interpretation of ground-surface lineaments (Evans,

1972). To do so, we performed a geomorphometric analysis of the same LiDAR-derived elevation model described above following Jordan (2003) based on the detection of ground curvatures. First, to enhance the visual detection of lineaments, four shaded reliefs were created with the insolation set to low inclinations (10°, 20°, 30° and 45° solar elevation angle, with three-times vertical exaggeration) and the sunshine azimuths perpendicular to the two known main tectonic fractures in the region: directions N40ºE to N45ºE and N140ºE to N160ºE (Ramli et al., 2010). Second, to identify the valleys and ridges, the drainage network was calculated using the D8 algorithm (Jenson and Domingue, 1988). Third, the degrees of the slope, aspect, and curvature were calculated at eight spatial scales (from 3 m x 3 m to 101 m × 101 m at intervals of 14 m) using the multiscale toolbox in the geomorphometric analysis in ArcGIS (Rigol-Sánchez et al., 2015). Finally, the fractures were located and digitized in a final lineament-like fracture map with the aid of field visits to validate the slope changes, an aerial orthoimage to validate the linear spatial patterns and geophysical methods under sands to validate the bedrock fracture zones (see section below).

2.2.3. VALIDATING FRACTURES WITH GEOPHYSICAL METHODS

Since underground electrical resistivity methods are costly and time-consuming, only two orthogonal profiles were performed on two lineaments to validate the fracture detection in the study area (Zhu et al., 2014; Schütze et al., 2012). The two chosen lineaments were not present in the geological map but were newly identified in this study and presented a linear distribution of *Ziziphus* patches. Each profile was randomly set perpendicular to its lineament. The results for only one of the profiles are shown, but both profiles provided enough evidence for fracture detection. SAS 4000 Terrameter equipment (ABEM, Inc.) was used to measure the underground resistivity, with an approximate resolution of ± 1μV. Data were acquired through four multiple channels with a set of electrodes and GRAD4S8/GRAD4 LX8 gradient protocols (ABEM, 2006). The gradient protocol uses a

Wenner-Schlumberger device with multiple channels (Dahlin and Zhou, 2006). The profiles were 80 m long, SW-NE oriented and had 1 m electrode spacing. Their position and elevation were measured with a Leica 1200+ differential GPS. The calculation of the inversion profiles was carried out with the RES2DINV software (v. 3.59, Geotomo Inc.) with the parameters set to the limitations of refinement model, standard minimum squares inversion, four nodes per unit electrode spacing, and the initial damping factor of 0.3. In addition, to determine the real depth of the resistivity of the materials, the gentle topography of the study area was calculated from a straight line of minimum squares and a distorted uniform grid for modelling the topography. The depth of the investigation index was calculated to test the consistency of the electrical resistivity tomography profiles (Oldenburg and Li 1999, Marescot et al., 2003). The most restrictive cutoff value of 0.1 was used to consider the data as highly reliable.

2.2.4. ANALYSIS OF ASSOCIATION OF ZIZIPHUS PATCHES WITH FRACTURES

To assess the spatial relationship between the *Ziziphus* patches and detected fractures, the average minimum distance was calculated between all centroids of the *Ziziphus* patches and fractures in PASSaGE 2 software (Rosenberg and Anderson, 2011). The analysis compares the minimum distances to fractures from the OBIA-mapped *Ziziphus* patches against the minimum distances to fractures from randomly distributed *Ziziphus* patches. To assess the significance of the difference in the average minimum distance, 999 maps of randomly distributed *Ziziphus* patches (with the same number of patches and areas as in the OBIA-map) were created, and the minimum distances of each iteration were recorded. To assess whether bedrock fractures would particularly facilitate the access to groundwater by smaller *Ziziphus* shrubs, *Ziziphus* patches (in the OBIA-map and in the random maps) were grouped into four size categories using the quartiles of the area, and significant differences of the average minimum distances among sizes were assessed using a Kruskal-Wallis test with multiple comparisons.

2.2.5. PROVING GROUNDWATER DEPENDENCE FROM NDVI DYNAMICS

To prove the dependence of *Ziziphus lotus* on groundwater in the study area, we compared the seasonal dynamics of the normalized difference vegetation index (NDVI) between pure 10 m x 10 m pixels of *Ziziphus* patches (42 pixels) and nearby vegetation (42 pixels) in relation to precipitation, following Eamus et al. (2015). For this, we computed the monthly NDVI maximum value composite from cloud-free pixels in the Sentinel-2A archive (Google Earth Engine, June 2015-June 2017). The capacity of maintaining green islands within a sea of browning senescent vegetation during the dry season was used to prove that *Z. lotus* was not subjected to the same degree of soil water deficit as the surrounding vegetation that does not have access to groundwater (Contreras et al., 2013).

3. RESULTS

3.1. MAP OF *ZIZIPHUS PATCHES*

The polygonal map of 1832 *Ziziphus* patches created from OBIA showed very high accuracy (Hellden's mean accuracy index = 0.90; Kappa index = 0.89; omission error = 0.08; and commission error = 0.02). The parameters for the best segmentation were Scale = 160, Shape = 0.6, and Compactness = 0.9, with a very high accuracy (ED2 index = 0.11; PSE = 0.10; NSR = 0.05) under non-hierarchical segmentation. From a total of 79779 segments, 1853 were classified as *Ziziphus*. Once the contiguous segments were merged, we identified 1832 *Ziziphus* patches, covering a total of 221195 m^2 in the study area. The average density within the extent of occurrence of *Ziziphus* in the study area was 6 patches/hectare. The smallest *Ziziphus* patch had an area of 11 m^2, and the largest patch reached 511 m^2. The mean size was 119 m^2, while the median size was 100 m^2 (Table 1). The population histogram (Figure 3) shows that the size of the *Ziziphus* patches is slightly skewed towards smaller

individuals, with the Z2 size-group (63 and 100 m^2) reaching the highest frequency (1.39 skewness index and 5.51 kurtosis index). Large individuals (e.g., larger than 300 m^2) were relatively scarce.

3.2. FRACTURE ZONES MAP

More than 20 km of lineaments were identified (Figure 4). The map showed relief structures in the area with high detail. The lineaments were drawn in the direction of N140ºE to N160ºE, i.e., parallel to the main known tectonic fractures (Goy and Zazo, 1986), although some structural features that were oriented N40ºE to N45ºE were also observed. The most appropriate geomorphometric maps were calculated using core size variables from 31 m × 31 m to 59 m x 59 m. The slope map calculated with a kernel of 31 m × 31 m indicated the position of four main structural features, and the map with a maximum curvature profile had a core of 59 m × 59 m, which further improved the detection of structural features in the direction of N140ºE to N160ºE and allowed for the extraction of some new structural features in the direction of N40ºE to N45ºE.

3.3. VALIDATION OF FRACTURE ZONES BY MEANS OF GEOPHYSICAL METHODS

Since the resistivity profiles showed similar results, we included only one profile here to save space (Figure 5). The profile showed intermediate resistive values (~1000 Ω · m), which were interrupted at 43 m by low resistivity values (~100 Ω · m) to the end of the NE side. Below this shallow layer, high resistivity values (~5000 Ω · m, from 3 to 8 m depth) were detected, which were modified between 23 and 39 m in length by the presence of fractures. The induced polarization profile showed high chargeability values linked with these fractures. The root mean square (RMS) obtained from the inversion profile was less than

10%, and the depth of the investigation index of 0.1 was located below the position of the fractures at approximately at 15 m a.s.l.

3.4. ASSOCIATION OF ZIZIPHUS PATCHES WITH FRACTURES

Ziziphus patches showed linear spatial patterns associated with fracture zones and tended to be more frequent near the fractures (61% of the population lived within 50 m from fractures; Figure 6 and Figure A1). The *Ziziphus* cover was 11%, and the *Ziziphus* density was 9 individuals per hectare within the first 50 m from fractures, while these values were 5% and 4 individuals per hectare in the rest of the extent of occurrence in the study area. The average minimum distance between *Ziziphus* patches and fractures was lower in the analysis of the OBIA-derived *Ziziphus* locations (52.16 m) than in the analysis of the random locations (163.78 m) in 99% of the 999 simulations (Table 2). In addition, smaller patches tended to be relatively more frequent near fractures than larger patches (Figure 6). Indeed, the average minimum distance of *Ziziphus* patches to fracture zones tended to increase with patch size (Table 2), and the smallest shrubs (Z1 group) were closest to the fracture zones, with an average of 43 m and a median of 33 metres. The distances to fractures of the smallest groups (Z1, Z2, and Z3 groups) were significantly smaller than the distances of the largest patches (Z4 group) (p-value = 0.05, n = 1832, Kruskal-Wallis test; Table 3).

3.5. PROVING GROUNDWATER DEPENDENCE FROM NDVI DYNAMICS

The seasonal dynamics of the normalized difference vegetation index (NDVI) of the *Ziziphus* patches differed from that of the nearby vegetation (Figure 7). The NDVI dynamics of the surrounding vegetation were coupled with precipitation and decoupled from temperature. Its growing season started in October after the first autumn rainfall, peaked in the middle of the winter when the temperatures were lowest and the rainfall was highest,

started senescence with the start of the dry season in May, and was the minimum during the summer drought. In contrast, the NDVI dynamics of the *Ziziphus* patches were typical of a winter-deciduous shrub, being more coupled to temperature than to precipitation. The *Ziziphus* growing season started in March when the temperatures increased after the winter, peaked in May (at the start of the dry season), and maintained relatively higher NDVI values than the surrounding vegetation throughout the summer drought, reaching minimum values during the autumn-winter.

4. DISCUSSION

The remotely sensed spatial distribution of shrubs and fractures helped us identify groundwater dependent ecosystems in drylands based on the spatial relationship between shrubs and fractures. First, by applying OBIA on a very-high-resolution orthoimage and a LiDAR-derived digital surface model, we produced a map of *Ziziphus* patches (1832 patches, 0.90 total accuracy). These *Ziziphus* patches were proven to maintain relatively high vegetation greenness during the summer drought while the surrounding vegetation was senescent, as revealed by the Sentinel-2A NDVI dynamics. Second, twenty kilometres of ground surface lineaments were also mapped based on the geomorphometric analysis of the LiDAR-derived elevation model. These surface lineaments were proven to represent subsurface fractures, as validated by geophysical electrical resistivity tomography. Altogether, our approach confirmed that the tendency of this phreatophyte to concentrate along fractures that facilitate its access to groundwater could help identify GDEs in semiarid environments.

4.1. ZIZIPHUS LOTUS ARBORESCENT MATORRAL HABITAT AS A GDE IN SE SPAIN

Vegetation greenness is known to be driven in this region by climate (mainly precipitation) but is modulated by lithology and vegetation (Cabello et al., 2012). The different dynamics and higher NDVI values maintained by *Z. lotus* during the summer drought confirmed that it behaves as a phreatophyte (Contreras et al., 2013) in SE Spain as it does in other regions (Gorai et al., 2010; Maraghni et al., 2014). This behaviour was also revealed by the tendency that all *Ziziphus* patches were concentrated along fractures. This can be explained as a facilitation to plant establishment since fractures form clay deposits with greater water holding capacities (Dekker and Hughson, 2014) and act as corridors to access groundwater (Colvin et al., 2003).

Our results also offered insight into the long-term environmental controls underlying the establishment of *Z. lotus* individuals in this semi-arid region. Smaller shrubs were closer together and more abundant along fractures than larger ones. This difference suggests that the establishment of larger and older individuals could have occurred in historical windows under wetter climatic conditions when fracture facilitation may not have been so critical. In this area, the largest shrubs could have established far from fractures during the Little Ice Age (200 years ago), when the temperature was lower, and the local rainfall was double the current amount (400 mm versus 200 mm) over the course of several decades (Martín-Rosales et al., 2007). This hypothesis, which should be tested in future research, agrees with the observed patterns of the patch sizes and the absolute lack of recruitment observed by the authors during the field preparation for an ongoing restoration project (ADAPTAMED LIFE14 CCA/ES/000612).

The confirmation that *Z. lotus* forms a GDE in the study area should lead to the creation of conservation and management plans under the WFD (see next section). Since the conservation of this priority habitat depends on the groundwater integrity, the local declines in the water table due to the increasing agriculture intensity and the subsequent seawater intrusion (Daniele et al., 2010; García et al., 2003), an irreversible short-term process (Chang et al., 2011) could be pushing this ecosystem to a local collapse (IUCN). These plans should extend beyond the park boundaries to ensure groundwater integrity within the park where the primary *Z. lotus* populations occur.

4.2. IMPLICATIONS UNDER THE HABITATS AND WATER FRAMEWORK DIRECTIVES IN EUROPE

Z. lotus arborescent matorral is a protected priority habitat (5220* of Habitats Directive) that is in serious decline in Europe (EEA, 2015). Unfortunately, the poor situation in SE Spain could become the common situation in Europe and North Africa, where many *Z. lotus* populations occur in coastal areas (Figure 1; Mücher et al., 2009) and are threatened by urban and agricultural sprawl, climate warming, aridification, and seawater intrusion (Ibáñez et al., 2015). The compulsory registration and protection (Articles 1 and 6 and Annex 4.5 of the WFD) of GDEs and the sexennial report on the conservation status of habitats (Art. 17 of Habitats Directive) should urgently include an assessment of the dependence of Habitat 5220* on groundwater.

Indeed, identifying GDEs is an increasingly demanded step in Europe (Boulton 2005, Kløve et al., 2011) for the protection and management of GDEs under the WFD (Articles 1 and 6) and a first step for the assessment of the hydrological ecosystem services (Carvalho-Santos et al. 2013) provided by GDEs. This identification becomes a challenge when groundwater is

not observed on the surface at any time of the year (UK TAG, 2012), and our approach can assist with this purpose.

4.3. POTENTIALS AND LIMITATIONS OF THIS APPROACH TO IDENTIFY GDES

The approach developed in this study that is based on the spatial relationship between the remotely sensed spatial distributions of phreatophytes and fractures offers several advantages for identifying potential GDEs. The method is simple, relatively low-cost, and non-destructive (neither to soil nor plants) (Eamus et al., 2006). Our method proved to be particularly successful in semi-arid regions, where the spatial distribution of phreatophytic vegetation is conditioned by root lengths (Canadell et al., 1996), aquifer depths (Hinsby et al., 2008), and the presence of bedrock fractures that facilitate the access to groundwater (Aich and Gross, 2008). In addition, the inertia in the spatial distribution of long-lived shrubs (see García and Zamora, 2003) such as *Z. lotus* minimizes the noise that external factors such as human disturbances of groundwater may have on the determination of the groundwater dependence of an ecosystem (Lautz, 2008). One of the limitations is that the collection of very-high-resolution imagery and digital elevation models can be difficult for some areas. However, as Guirado *et al.* (under review) proved, the use of OBIA and convolutional neural networks on freely available Google Earth high-resolution images offers very high accuracies to detect phreatophytic shrubs such as *Z. lotus*. Even if a fine resolution fracture map was not available, the mere detection of spatial lineaments in phreatophytic plants could be used as an indirect indicator of potential groundwater resources (even more if the plant lineaments agree with the direction of the main regional faults) to support further evaluations.

5. CONCLUSION

This work provides a remote-sensing-based approach for the increasingly demanded identification of groundwater dependent ecosystems (GDEs) as a means for their protection and management (Boulton 2005, Kløve et al., 2011). The spatial association between the remotely sensed spatial distribution of *Ziziphus lotus* shrubs and bedrock fractures helped identify a groundwater dependent ecosystem in a dryland where the surface expressions of groundwater are not obvious. The majority (61%) of the *Z. lotus* patches, particularly the smallest ones, were concentrated within 50 m from fractures, which facilitate their access to groundwater. Electrical resistivity tomography was used to validate the identified fractures and the seasonal dynamics of the normalized difference vegetation index to prove that *Z. lotus* maintained higher greenness during the summer drought and was less coupled with precipitation than the nearby non-phreatophytic vegetation. The proposed approach used to identify GDEs requires only very high spatial resolution RGB orthoimagery for shrub mapping (e.g., from Google Earth; see Guirado et al., 2017), an accurate fracture map (e.g., derived from a digital elevation model), and spatial statistics to assess the association between shrubs and fractures. The already reported decline of Habitat 5220* in Europe (EEA, 2015), which is an "Arborescent matorral with *Ziziphus*", and our proven dependence of the main European *Z. lotus* population on groundwater, indicate the need for its urgent assessment under the Water Framework Directive to comply with the compulsory registration and protection of GDEs (Articles 1 and 6 and Annex 4.5 of WFD). Such assessment must eventually lead to the designation of influence areas for their subsequent protection (Boulton, 2005; Kløve et al., 2014a).

ACKNOWLEDGMENTS

We would like to thank the two reviewers for their comments and suggestions that served to improve this work. This research was developed in The Arid Iberian South East LTSER Platform (LTER_EU_ES_027). We are grateful to the Andalusian Center for the Assessment and Monitoring of Global Change (CAESCG) for the orthoimages and LiDAR data, and to the Department of Geodynamics in University of Granada for the electrical resistivity tomography data. Financial Support was given by the European LIFE Project ADAPTAMED (LIFE14 CCA/ES/000612), (CGL2016-80687-R AEI/FEDER) DAMAGE, Spanish MINECO (grant JC2015-00316 and project CGL2014-61610-EXP), and to ERDF. The work was also partially developed as part of project ECOPOTENTIAL, which received funding from the European Union's Horizon 2020 Research and Innovation Program under grant agreement No. 641762.

REFERENCES

ABEM (2006). ABEM Terrameter SAS 1000/4000 Instructions Manual.

Aich, S., and Gross, M. R. (2008). Geospatial analysis of the association between bedrock fractures and vegetation in an arid environment. *International Journal of Remote Sensing*, *29* (23), 6937-6955.

Barron, O., Silberstein, R., Ali, R., Donohue, R., McFarlane, D.J., Davies, P., Hodgson, G., Smart, N., and Donn, M. (2012). Climate change effects on water-dependent ecosystems in south-western Australia. *Journal of Hydrology*, *434*, 95-109.

Boulton, A. J. (2005). Chances and challenges in the conservation of groundwaters and their dependent ecosystems. *Aquatic Conservation: marine and freshwater ecosystems*, *15*(4), 319-323.

Brown, J., Bach, L., Aldous, A., Wyers, A., and DeGagné, J. (2010). Groundwater-dependent ecosystems in Oregon: an assessment of their distribution and associated threats. *Frontiers in Ecology and the Environment*, *9*(2), 97-102.

Burnett, C., and Blaschke, T. (2003). A multi-scale segmentation/object relationship modelling methodology for landscape analysis. *Ecological modelling*, *168*(3), 233-249.

Cabello, J., Alcaraz-Segura, D., Ferrero, R., Castro, A. J., and Liras, E. (2012). The role of vegetation and lithology in the spatial and inter-annual response of EVI to climate in drylands of Southeastern Spain. *Journal of Arid Environments*, *79*, 76-83.

Canadell, J., Jackson, R. B., Ehleringer, J. B., Mooney, H. A., Sala, O. E., and Schulze, E. D. (1996). Maximum rooting depth of vegetation types at the global scale. *Oecologia*, *108*(4), 583-595.

Chamizo, S., Rodríguez-Caballero, E., Cantón, Y., Asensio, C., and Domingo, F. (2015). Penetration resistance of biological soil crusts and its dynamics after crust removal: Relationships with runoff and soil detachment. *Catena*, *126*, 164-172.

Chang, S. W., Clement, T. P., Simpson, M. J., and Lee, K. K. (2011). Does sea-level rise have an impact on saltwater intrusion?, *Advances in Water Resources*,*34*(10), 1283-1291.

Clinton, N., Holt, A., Scarborough, J., Yan, L., and Gong, P., (2010). Accuracy assessment measures for object-based image segmentation goodness. *Photogrammetric Engineering and Remote Sensing*, *76* (3), 289-299.

Cohen, J. (1968). Weighted kappa: Nominal scale agreement provision for scaled disagreement or partial credit. *Psychological bulletin*, *70*(4), 213.

Colvin C., Le Maitre D., and Hughes S. (2003). *Assessing terrestrial groundwater dependent ecosystems in South Africa*. Report No. 1090-2/2/03. Water Research Commission, Pretoria.

Contreras, S., Alcaraz-Segura, D., Scanlon, B., and Jobbágy, E. G. (2013). Detecting ecosystem reliance on groundwater based on satellite-derived greenness anomalies and temporal dynamics. In: *Earth Observation of Ecosystem Services*; Alcaraz-Segura, D., di Bella, C.M., Straschnoy, J.V. (Ed.), CRC Press: Boca Raton, FL, USA, 2013; 283-302.

Dahlin, T. and Zhou, B. (2006). Multiple-gradient array measurements for multichannel 2D resistivity imaging. *Near Surface Geophysics*, *4*(2), 113-123.

Daniele, L., Sola, F., Izquierdo, A. V., and Bosch, A. P. (2010). Coastal aquifers and desalination plants: some interpretations to new situations. In *Conference on Water Observation and Information System for Decision Support. Balwois*, *Ohrid, Republic of Macedonia*, No. 25, 8p.

Definiens, A.G. (2009). Definiens Developer 7 user guide. *München: Definiens AG*.

Dekker, F. J., and Hughson, D. L. (2014). Reliability of ephemeral montane springs in Mojave National Preserve, California. *Journal of Arid Environments*,*111*, 61-67.

Eamus, D., Froend, R., Loomes, R., Hose, G., and Murray, B. (2006). A functional methodology for determining the groundwater regime needed to maintain the health of groundwater-dependent vegetation. *Australian Journal of Botany 54*, 97-114

Eamus, D., Zolfaghar, S., Villalobos-Vega, R., Cleverly, J., and Huete, A. (2015). Groundwater-dependent ecosystems: recent insights from satellite and field-based studies. *Hydrology and Earth System Sciences*, *19*(10), 4229-4256.

EEA, European Environment Agency *European topic centre on biological diversity*. (2015). Reporting Under Article 17 of the Habitats Directive (Period 2007–2012). Outcomes From the Article 17 Reports. EEA, Brussels (https://bd.eionet.europa.eu/activities/Reporting/Article_17 (accessed 8th, Nov. 2017)).

Esch, T., Thiel, M., Bock, M., Roth, A., and Dech, S. (2008). Improvement of image segmentation accuracy based on multiscale optimization procedure. *Geoscience and Remote Sensing Letters, IEEE*, *5*(3), 463-467.

Evans, I.S. (1972). *General geomorphometry, derivatives of altitude and descriptive statistics.* In: Chorley, R.J. (Ed.), Spatial Analysis in Geomorphology. Methuen and Co. Ltd., London, UK, 17-90.

García, J.P., Sánchez Caparós, A., Castillo, E., Marín, I., Padilla, A. and Rosso, J.I. (2003). *Hidrogeoquímica de las aguas subterráneas en la zona de Cabo de Gata.* In: López-Geta, J.A., Gómez, J., de la Orden, J.A., Ramos, J., Rodríguez, L (Ed.) Tecnología de la intrusión de agua de mar en acuíferos costeros: países mediterráneos, IGME, Madrid. 413- 422.

Garcia, D., and Zamora, R. (2003). Forum Persistence , multiple demographic strategies and conservation in long-lived Mediterranean plants. *Journal of Vegetation Science*, 14, 921–926.

Goy, J. L., and Zazo, C. (1983). Los piedemontes cuaternarios de la región de Almería (España). Análisis morfológico y relación con la neotectónica. *Cuadernos do Laboratorio Xeoloxico de Laxe*, *5*, 397-419.

Gorai, M., Maraghni, M., and Neffati, M. (2010). Relationship between phenological traits and water potential patterns of the wild jujube Ziziphus lotus (L.) Lam. in southern Tunisia. *Plant Ecology & Diversity*, *3*(3), 273-280.

Goy, J.L., Zazo, C. (1986). Synthesis of the Quaternary in the Almería littoral neotectonic activity and its morphologic features, western Betics, Spain. *Tectonophysics, 130*, 259-270.

Guirado, E., Tabik, S., Alcaraz-Segura, D., Cabello, J., and Herrera, F. (2017) Deep-learning versus OBIA for scattered shrub detection with Google Earth imagery: *Ziziphus lotus* as case study. *Remote Sensing*. 9(12), 1220.

Hinsby, K., de Melo, M. T. C., and Dahl, M. (2008). European case studies supporting the derivation of natural background levels and groundwater threshold values for the protection of dependent ecosystems and human health. *Science of the Total Environment*, *401*(1), 1-20.

Howard, J., and Merrifield, M. (2010). Mapping groundwater dependent ecosystems in California. *PLoS One*, *5*(6), e11249.

Ibáñez, J. J., Pérez-Gómez, R., Oyonarte, C., and Brevik, E. C. (2015). Are There Arid Land Soilscapes in Southwestern Europe? *Land Degradation & Development*, *26*(8), 853-862.

Jenson, S.K. and Domingue, J.O. (1988). Extracting topographic structure from digital elevation data for Geographic Information System analysis. *Photogrammetric Engineering and Remote Sensing*, *54*(11), 1593-1600.

Jordan, G. (2003). Morphometric analysis and tectonic interpretation of digital terrain data: A case study. *Earth Surface Processes and Landforms, 28*(8), 807-822.

Kløve, B., Allan, A., Bertrand, G., Druzynska, E., Ertürk, A., Goldscheider, N., Henry, S., Karakaya, N., Karjalainen, T. P., Koundouri, P., Kupfersberger, H., Kvœrner, J., Lundberg, A., Muotka, T., Preda, E., Pulido Velázquez, M., and Schipper, P. (2011).

Groundwater dependent ecosystems. Part II. Ecosystem services and management in Europe under risk of climate change and land use intensification. *Environmental Science and Policy, 14*(7), 782-793.

Kløve, B., Balderacchi, M., Gemitzi, A., Hendry, S., Kværner, J., Muotka, T., and Preda, E. (2014a). Protection of groundwater dependent ecosystems: current policies and future management options. *Water Policy, 16*(6), 1070-1086.

Kløve, B., Ala-Aho, P., Bertrand, G., Gurdak, J. J., Kupfersberger, H., Kværner, J., Muotka, T., Mykrä, H., Preda, E., Rossi, P., Uvo, C. B., Velasco, E., and Pulido-Velazquez, M. (2014b). Climate change impacts on groundwater and dependent ecosystems. *Journal of Hydrology, 518*, 250-266.

Lagarde, F., Louzizi, T., Slimani, T., El Mouden, H., Kaddour, K. B., Moulherat, S., and Bonnet, X. (2012). Bushes protect tortoises from lethal overheating in arid areas of Morocco. *Environmental Conservation, 39*(02), 172-182.

Lang, S., and Langanke, T. (2006). Object-based mapping and object-relationship modeling for land use classes and habitats. *Photogrammetrie Fernerkundung Geoinformation*, 1, 5-18.

Lautz, L. K. (2008). Estimating groundwater evapotranspiration rates using diurnal water-table fluctuations in a semi-arid riparian zone. *Hydrogeology Journal, 16*(3), 483-497.

Le Houérou, H.N. (2006). Agroforestry and silvopastoralism: The role of trees and shrubs (Trubs) in range rehabilitation and development. *Science et changements planétaires / Sécheresse 17*(1), 343-348.

Liu, Y., Bian, L., Meng, Y., Wang, H., Zhang, S., Yang, Y., Xao, X., and Wang, B. (2012). Discrepancy measures for selecting optimal combination of parameter values in object-based image analysis. *ISPRS Journal of Photogrammetry and Remote Sensing, 68*, 144-156.

Maraghni, M., Gorai, M., Neffati, M., and Van Labeke, M. C. (2014). Differential responses to drought stress in leaves and roots of wild jujube, Ziziphus lotus. *Acta physiologiae plantarum, 36*(4), 945-953.

Marescot, L., Loke, M.H., Chapellier, D., Delaloye, R., Lambiel, C. and Reynard, E. (2003). Assessing reliability of 2D resistivity imaging in mountain permafrost studies using the depth of investigation index method. *Near Surface Geophysics, 1*(2), 57-67.

Martín-Rosales, W., Pulido-Bosch, A., Vallejos, Á., Gisbert, J., Andreu, J. M., and Sánchez-Martos, F. (2007). Hydrological implications of desertification in southeastern Spain/Implications hydrologiques de la désertification dans le sud-est de l'Espagne. *Hydrological Sciences Journal/Journal des Sciences Hydrologiques*, *52*(6), 1146-1161.

Mücher, C. A., Hennekens, S. M., Bunce, R. G., Schaminée, J. H., and Schaepman, M. E. (2009). Modelling the spatial distribution of Natura 2000 habitats across Europe. *Landscape and urban planning*, *92*(2), 148-159.

Münch, Z. and Conrad, J. (2007). Remote sensing and GIS based determination of groundwater dependent ecosystems in the Western Cape, South Africa. *Hydrogeology Journal*, *15*(1), 19-28.

Murray, B. B. R., Zeppel, M. J., Hose, G. C., and Eamus, D. (2003). Groundwater‐dependent ecosystems in Australia: It's more than just water for rivers. *Ecological Management & Restoration*, *4*(2), 110-113.

Naumburg, E., Mata-Gonzalez, R., Hunter, R.G., Mclendon, T., and Martin, D.W. (2005). Phreatophyte vegetation and groundwater fluctuations: a review of current research and application of ecosystem response modeling with an emphasis on Great Basin vegetation. *Environmental Management*, *35*(6), 726-740.

Oldenburg, D.W. and Li, Y. (1999). Estimating depth of investigation in dc resistivity and IP surveys. *Geophysics*, *64*(2), 403-416.

Oyonarte, C., Rey, A., Raimundo, J., Miralles, I., and Escribano, P. (2012). The use of soil respiration as an ecological indicator in arid ecosystems of the SE of Spain: Spatial variability and controlling factors. *Ecological Indicators*, *14*(1), 40-49.

Pérez-Hoyos, I. C., Krakauer, N. Y., Khanbilvardi, R., and Armstrong, R. A. (2016). A review of advances in the identification and characterization of groundwater dependent ecosystems using geospatial technologies. *Geosciences*, *6*(2), 17.

Ramli, M., Yusof, N., Yusoff, M., Juahir, H., and Shafri, H. (2010). Lineament mapping and its application in landslide hazard assessment: a review. *Bulletin of Engineering Geology and the Environment*, *69*, 215–233.

Rigol-Sánchez, J.P., Stuart, N., and Pulido-Bosch, A. (2015). ArcGeomorphometry: A toolbox for geomorphometric characterisation of DEMs in the ArcGIS environment. *Computers and Geosciences, 85*, 155–163.

Rivas Goday, S., and Bellot, F. (1944). Las formaciones de Zizyphus lotus (L.) Lam., en las dunas del Cabo de Gata. *Anal. Inst. Esp. Edaf. Fisiol. Veg*, *3*, 109-126.

Rodríguez J. (2016). Estructura poblacional de Ziziphus lotus (L.) Lam. (L.) en el Parque Natural de Cabo de Gata-Níjar mediante teledetección usando análisis orientado a objetos de ortoimágenes y LiDAR. *University of Granada, BOT-4* (1/2).

Rosenberg, M.S. and Anderson, C.D. (2011). PASSaGE: pattern analysis, spatial statistics and geographic exegesis. Version 2. *Methods in Ecology and Evolution*, *2*(3), 229-232.

Schütze, C., Vienken, T., Werban, U., Dietrich, P., Finizola, A., and Leven, C. (2012). Joint application of geophysical methods and Direct Push-soil gas surveys for the improved delineation of buried fault zones. *Journal of Applied Geophysics*, *82*, 129-136.

Sola, F., Daniele, L., Vallejos-Izquierdo, A., Sánchez-Martos, F., Urizar, R. and Pulido-Bosch, A. (2007). Influencia de la desaladora de Rambla Morales (Almería) sobre las características hidrogeológicas del acuífero del que se abastece. En: Los acuíferos costeros: retos y soluciones, 997-1004.

Syed, S., Dare, P. and Jones, S. (2005). Automatic classification of land cover features with high resolution imagery and lidar data: an object-oriented approach. In *Proceedings of SSC2005 spatial intelligence, innovation and praxis: the national biennial Conference of the Spatial Sciences Institute*, Melbourne: Melbourne: Spatial Science Institute, 512-522.

Tirado, R. (2009). 5220 Matorrales arborescentes con *Ziziphus lotus* (*). En: VV.AA., Bases ecológicas preliminares para la conservación de los tipos de hábitat de interés comunitario en España. *Ministerio de Medio Ambiente, y Medio Rural y Marino*, 68.

Tirado R. and Pugnaire F. (2003). Shrub spatial aggregation and consequences for reproductive success. *Oecologia, 136*, 296-301

Tirado R. and Pugnaire F. (2005). Community structure and positive interactions in constraining environments. *OIKOS, 111*, 437-444.

UK TAG; *UK Technical Advisory Group on the Water Framework Directive*. (2012). Technical report on groundwater-dependent terrestrial ecosystem (GWDTE) threshold values. *Final Consultation Document*.

Walter, H. and Breckle, S.W. (1986) *Ecological systems of the geobiosphere*. Springer, Berlin, Heidelberg.

Witharana, C., and Civco, D. L. (2014). Optimizing multi-resolution segmentation scale using empirical methods: Exploring the sensitivity of the supervised discrepancy measure Euclidean distance 2 (ED2). *ISPRS Journal of Photogrammetry and Remote Sensing, 87*, 108-121.

Zhu, T., and Zhou, J. G. (2014). Detection of a Buried Fault in Yuxi Basin Using ERT: Implications to New Urban Planning of Yuxi City, Yunnan Province, China. In *Advanced Materials Research, 831*, 228-231.

Revised 15 November 2017

Table 1. Size classes of *Ziziphus* patches. The classes were created using quartiles (area increases from Z1 to Z4). The mapping of 1982 patches was based on object-based image analysis of a 10 cm x 10 cm RGB orthoimage and a 1 m x 1 m LiDAR-derived digital surface model that were simultaneously acquired in August 2011 in the semi-arid coastal plain of *Cabo de Gata-Níjar* Natural Park, SE Spain. SD: standard deviation.

***Ziziphus* patch area (m^2)**	**Size class**				
	Z1	**Z2**	**Z3**	**Z4**	**All**
Minimum	11	64	101	159	11
Maximum	63	100	158	511	511
Average	44	81	126	228	119
SD	12	11	17	66	26

Table 2. Observed *versus* random distances of *Ziziphus* patches to fractures. *Ziziphus* patches were closer than random points to fractures, and the distance to fractures decreased from the largest (Z4) to the smallest (Z1) size class (see sizes in Table 1). The distances were calculated using average minimum distance (AMD) analysis from each *Ziziphus* patch centroid to the closest fracture in the semi-arid coastal plain of *Cabo de Gata-Níjar* Natural Park, SE Spain. SD: standard deviation

Distance of *Ziziphus* patches to fracture zones (m)	Z1	Z2	Z3	Z4	All
Observed Median AMD	33.0	39.0	42.5	50.0	41.1
Observed Average AMD	43.1	50.8	52.9	61.7	52.1
Observed SD of AMD	1.8	2.1	1.9	2.2	2.0
Random Average AMD	116.7	130.6	157.0	136.4	135.2
Random SD of AMD	6.4	7.5	8.6	7.3	7.5

Table 3. Differences between size classes in the average minimum distance (AMD) from *Ziziphus* patches to fractures in the semi-arid coastal plain of *Cabo de Gata-Níjar* Natural Park, SE Spain. The size increases from Z1 to Z4 (see Table 1). The distance from the largest patches (Z4) to fractures was significantly longer than that for the rest of the classes (Z1, Z2, Z3). The significance of the AMD difference was evaluated using a Kruskal-Wallis multicomparison test (p-value 0.05; n=916).

AMD to faults comparisons	**Observed difference in AMD (m)**	**Critical difference in AMD (m)**	**Significant difference of AMD**
Z1-Z2	58.2	92.9	false
Z1-Z3	71.1	91.1	false
Z1-Z4	183.7	92.2	true
Z2-Z3	12.9	92.2	false
Z2-Z4	125.4	93.3	true
Z3-Z4	112.5	91.5	true

Table 4. Accuracy metrics used to assess the overlap between the field-digitized reference polygons and the OBIA-obtained segments: Euclidean distance v.2 (ED2), potential segmentation error (PSE), and number-of-segments ratio (NSR).

Equation	**Description**
Eq. 1: $PSE = \frac{\sum\lvert s_i - r_k\rvert}{\sum\lvert r_k\rvert}$	PSE assesses the geometric or contour coincidence. r_k is the area of the field-digitized polygons in the reference dataset, s_i is the overestimated area of the OBIA-obtained segments, and i and k vary from 1 to the number of polygons and segments, respectively.
Eq. 2: $NSR = \frac{abs(m-v)}{m}$	NSR assesses the arithmetic or surface coincidence. abs is the absolute value of the difference between the number of field-digitized polygons (m) and the number of OBIA-obtained segments (v).
Eq. 3: $ED2 = \sqrt{(PSE)^2 + (NSR)^2}$	ED2 comprises both PSE and NSR accuracies.

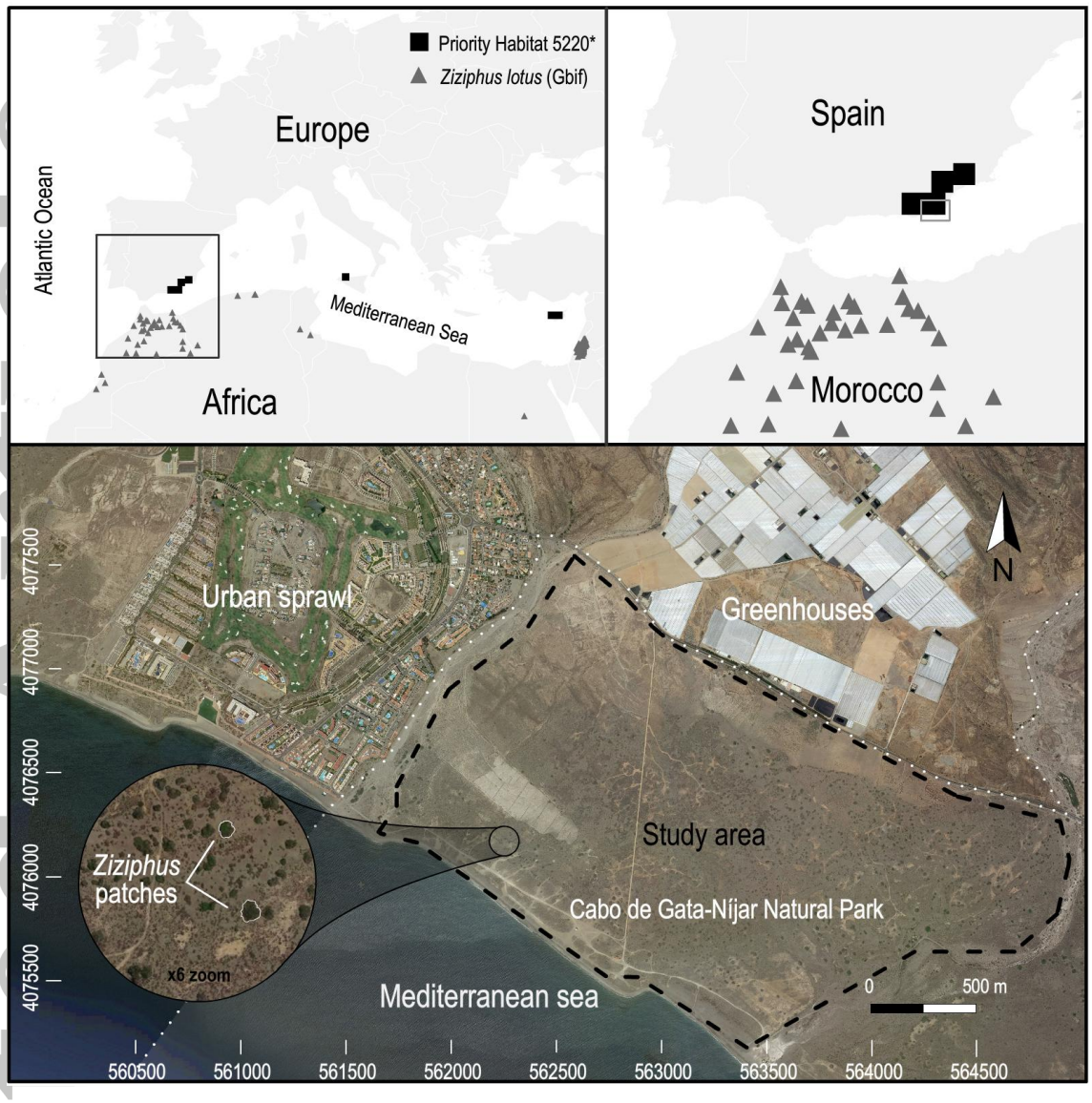

Figure 1. Distribution of *Ziziphus lotus* in the study area. The upper panels show, the official distribution of "Priority Habitat 5220* - Arborescent Shrub with *Ziziphus*" in Europe (black squares) (European Union Directive 92/43/EEC; EEA, 2015) and the records of *Ziziphus lotus* contained in the GBIF (Global Biodiversity Information Facility, December 2016) in North Africa and the Middle East (grey triangles). The lower panel shows the study area (black-dash polygon) in the semi-arid coastal plain of *Cabo de Gata-Níjar* Natural Park (white-points polygon), SE Spain, which was surrounded by greenhouses and urban sprawl in 2016. The zoomed image shows *Ziziphus* patches surrounded by sparse vegetation and bare soil in 2016 (orthoimage from Google Earth). The coordinate system is ETRS89 UTM 30N.

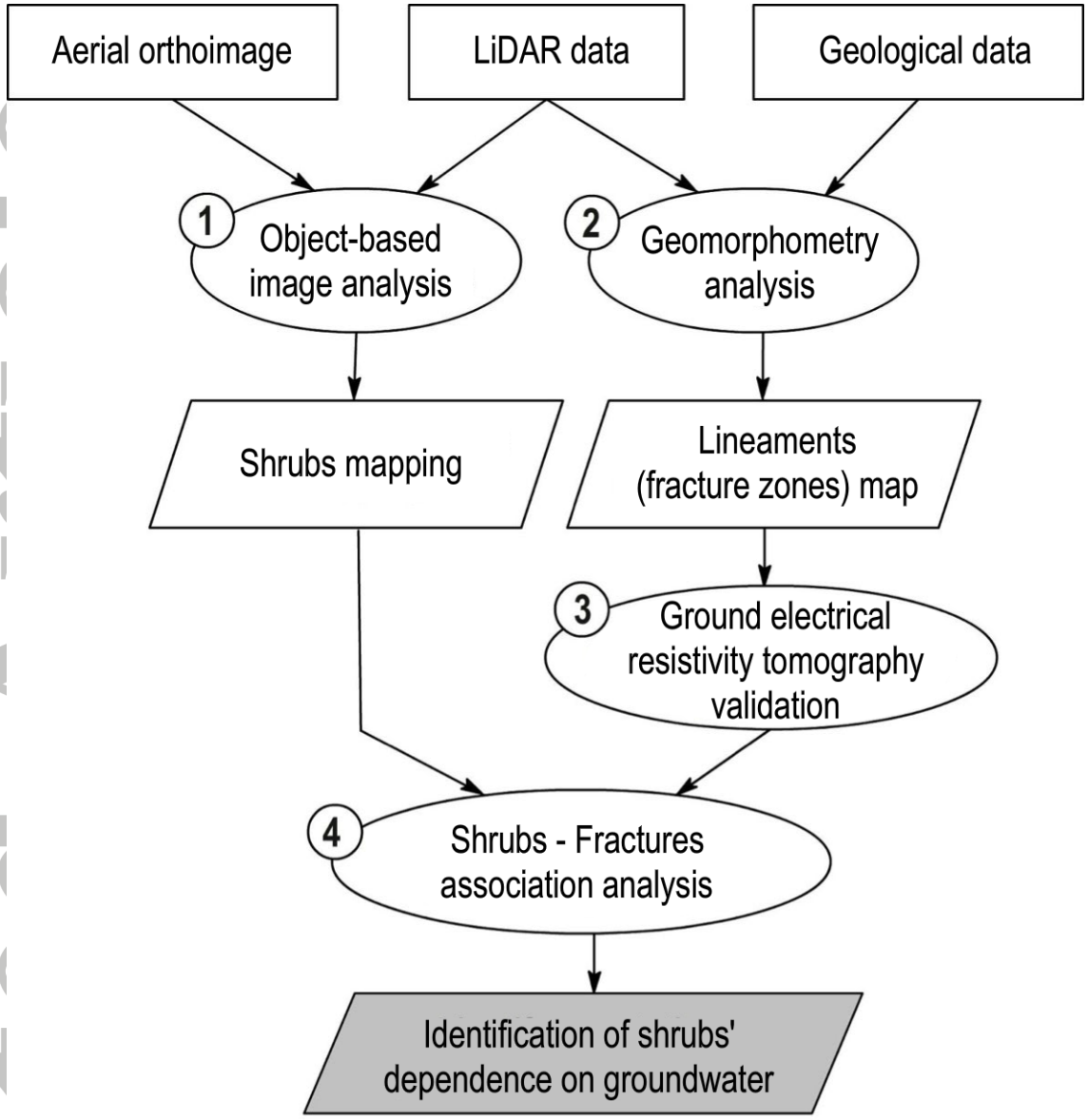

Figure 2. Proposed workflow to determine the dependence of phreatophytic arborescent shrubs on groundwater in semi-arid regions. The data sources are in rectangles, the processes and tools are in ovals, and the results are in trapezoids.

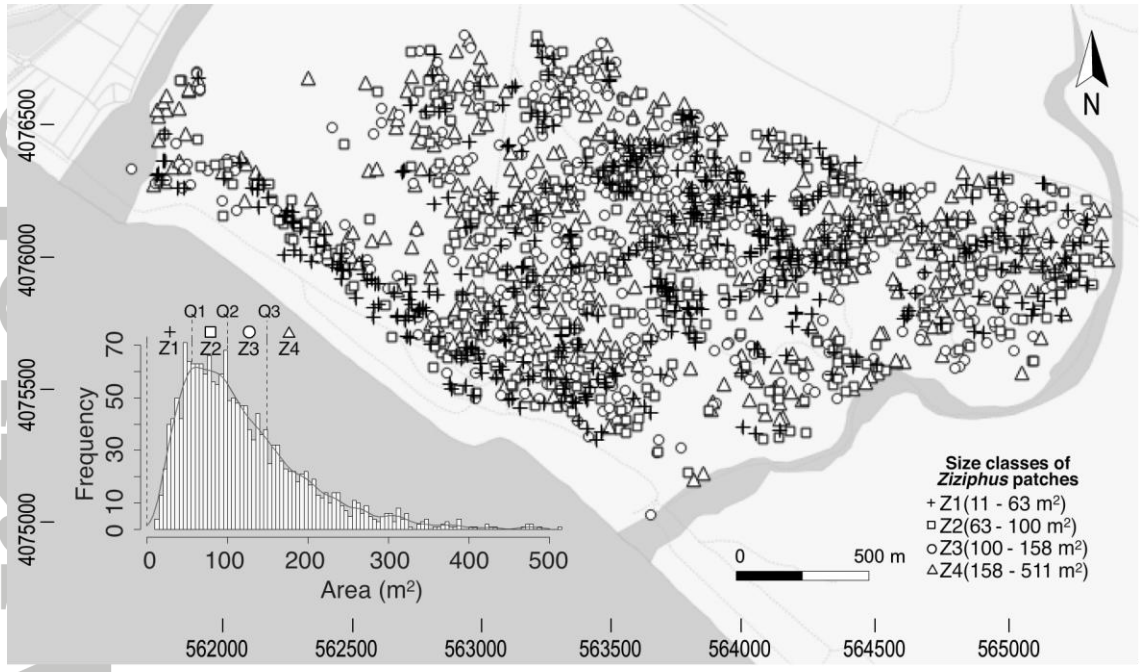

Figure 3. Map of the *Ziziphus* patches differentiated in four size classes. The mapping was based on OBIA of a 10 cm x 10 cm RGB orthoimage and a 1 m x 1 m LiDAR-derived digital surface model that were simultaneously acquired in August 2011. The inset histogram shows the frequency distribution of the patch sizes and the quartiles used to separate them into four size classes. The lineaments of the *Ziziphus* patches can be visually discerned mainly along and perpendicular to the coast and to the E and W wadis (in grey) that limit the study area (dashed black polygon). The coordinate system is ETRS89 UTM 30N.

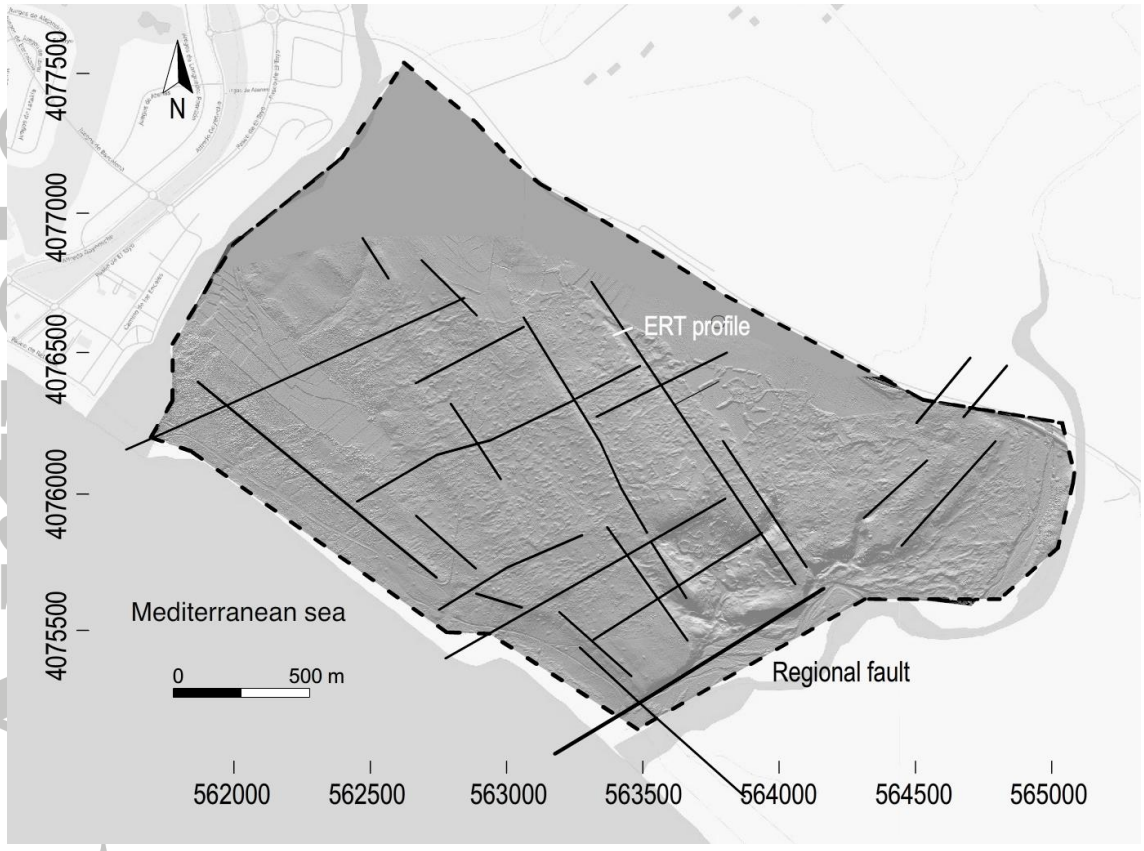

Figure 4. Map of the lineaments, such as fractures (black lines), detected from the geomorphometric analysis of the LiDAR-derived digital elevation model. The white line shows the SW-NE 80 m electrical resistivity tomography (ERT) profile (Figure 5). The thick black line in the SW shows the major regional fault that separates the Torre García local aquifer from the Hornillo-Cabo de Gata regional aquifer. The coordinate system is ETRS89 UTM 30N.

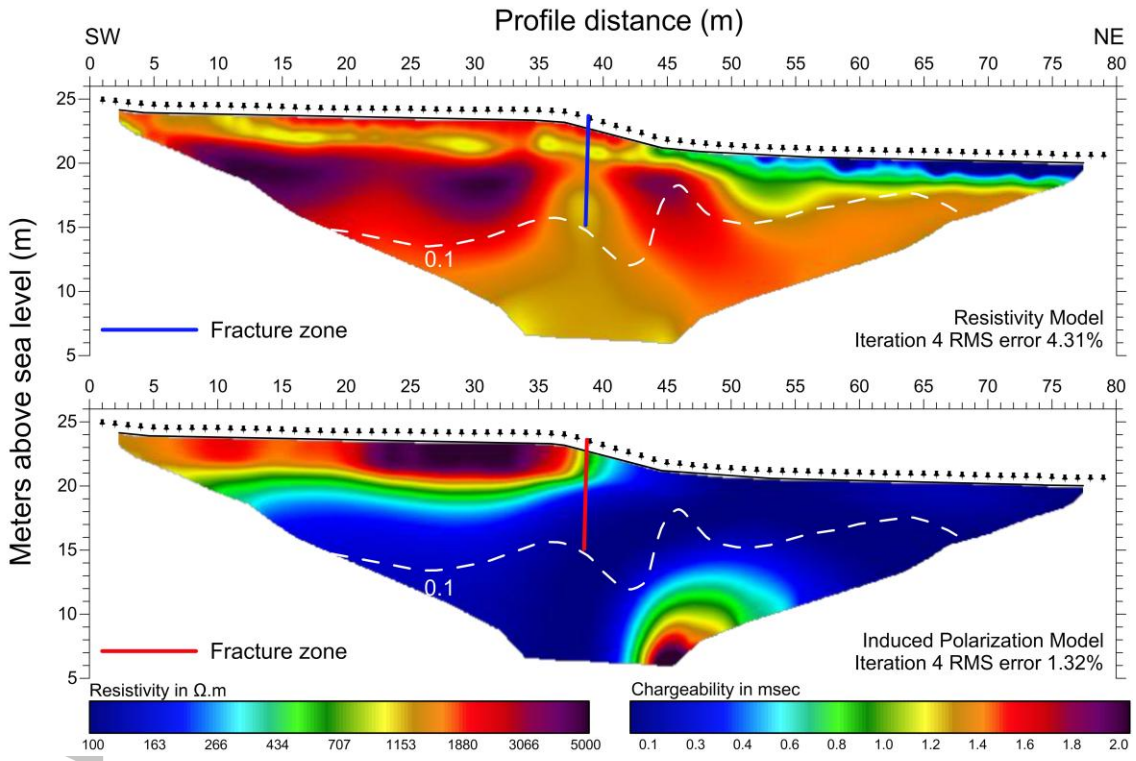

Figure 5. Profile 80 metres in length orthogonal to a fracture (see location in Figure 4). The abrupt changes in the inversion model of electrical resistivity tomography (top) and in the induced polarization or chargeability (bottom) led us to locate the fracture zone marked by the vertical lines. The fracture was detected using geomorphometric analysis of the LiDAR-derived digital elevation model and resistivity tomography. The results are confident from the surface down to the white dashed line that indicates the *0.1 depth of investigation* value.

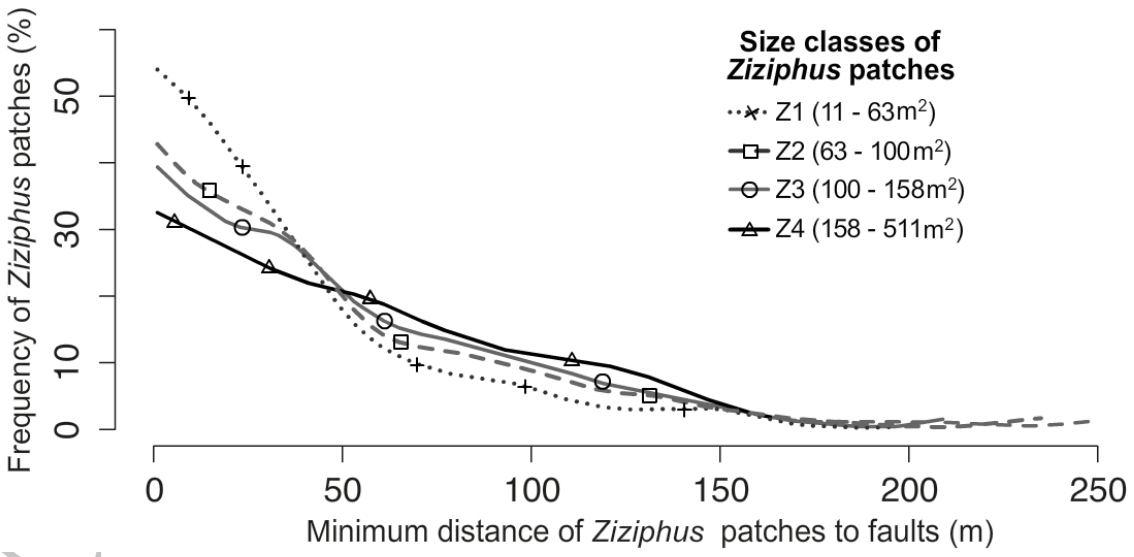

Figure 6. Decrease in the abundance (frequency) of *Ziziphus* patches (*per* size class) as the minimum distance to fracture zones increases. The 1832 mapped *Ziziphus* patches were separated using quartiles into four size classes of 458 polygons each (size increases from Z1 to Z4, Table 1) to illustrate how smaller patches were more abundant near fractures than larger patches. A total of 61% of the *Ziziphus* patches occurred within 50 m from faults. The *Ziziphus* cover was 11%, and *Ziziphus* density was 9 individuals per hectare in the first 50 m from fractures, while these values were 5% and 4 individuals per hectare in the rest of the extent of occurrence in the study area.

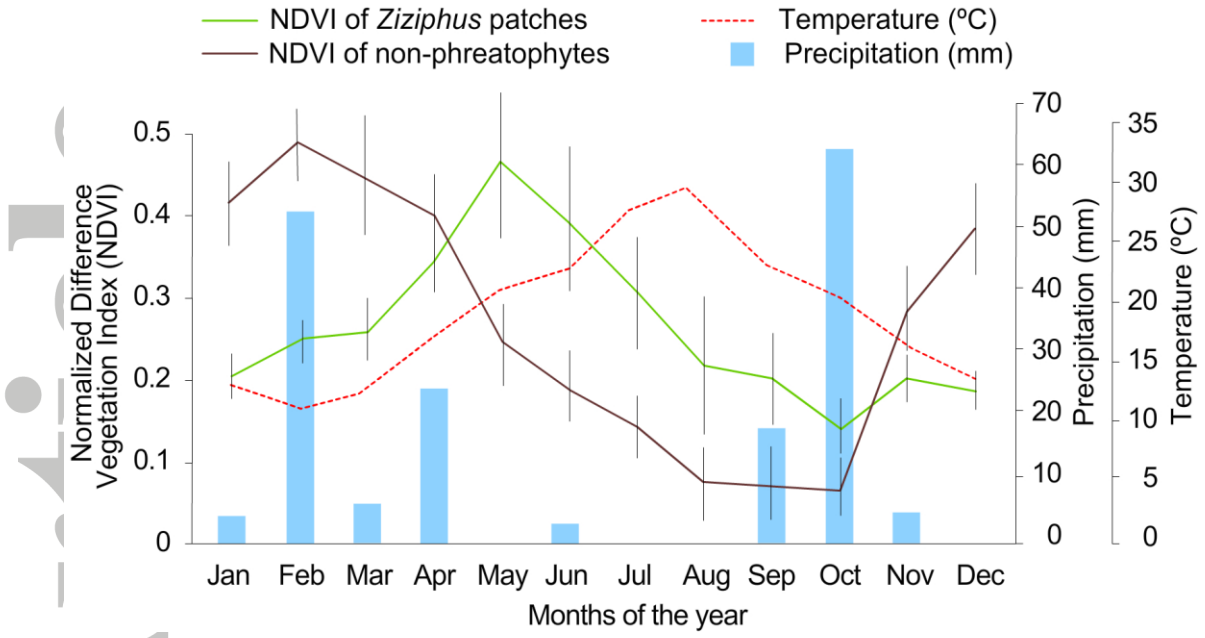

Figure 7. Contrast between the seasonal dynamics of the normalized difference vegetation index (NDVI) of *Ziziphus lotus* patches and the nearby non-phreatophytic vegetation. The NDVI was obtained from Sentinel-2A satellite images from June 2015 to June 2017 for cloud-free pure 10 m x 10 m pixels of *Ziziphus* patches (42 pixels) and nearby vegetation (42 pixels). Precipitation and temperature data were obtained from the Almería airport meteorological station, which is close to the study area, for the same period. The NDVI of the non-phreatophytic vegetation was coupled with precipitation while the *Ziziphus* patches maintained higher NDVI during the summer drought.

APPENDIX

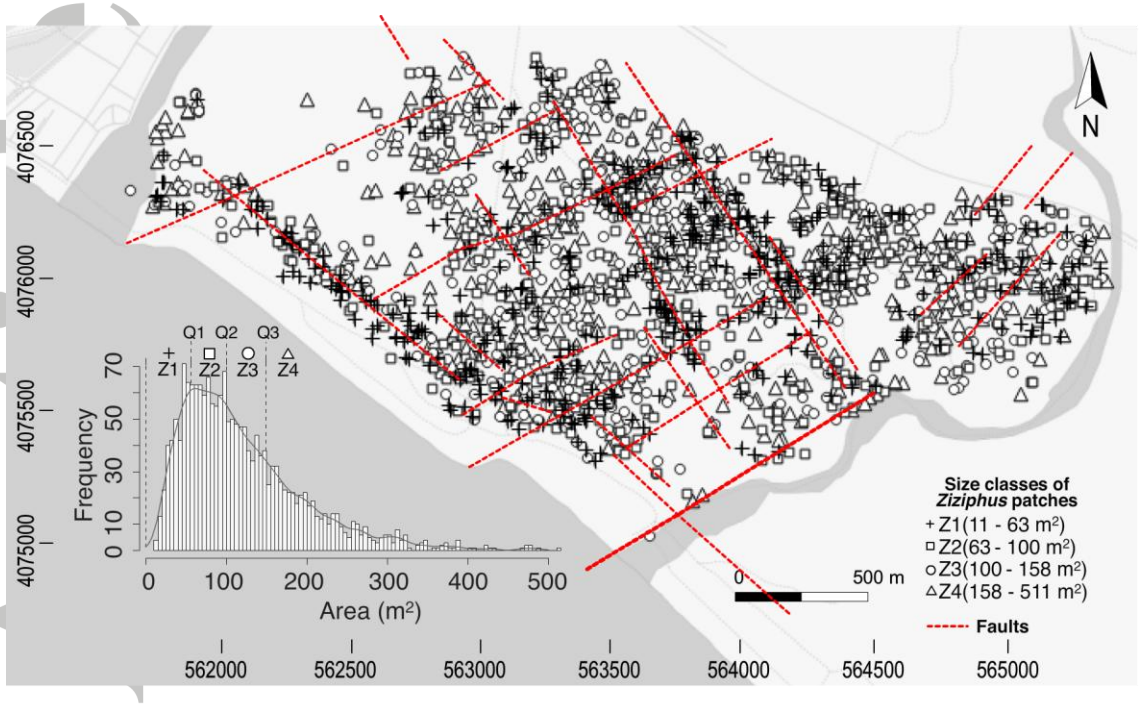

Figure A1. Map of *Ziziphus* patches differentiated into four size classes and the map of the lineaments, such as fractures (dotted red line), detected from the geomorphometric analysis of the LiDAR-derived digital elevation model. The coordinate system is ETRS89 UTM 30N.